Microstructuring of 2D perovskites via ion-exchange fabrication

Grimaldi, G.; Antony, L.S.D.; Helmbrecht, L.; van der Weijden, A.; van Dongen, S.W.; Schuringa, I.; Borchert, J.; Alarcón-Lladó, E.; Noorduin, W.L.; Ehrler, B.

DOI
10.1063/5.0065070

Publication date
2021

Document Version
Final published version

Published in
Applied Physics Letters

Applied Physics Letters ARTICLE scitation.org/journal/apl

Microstructuring of 2D perovskites via ion-exchange fabrication

Cite as: Appl. Phys. Lett. **119**, 223102 (2021); doi: 10.1063/5.0065070
Submitted: 29 July 2021 · Accepted: 12 November 2021 ·
Published Online: 29 November 2021

G. Grimaldi,[1,2] L. S. D. Antony,[2] L. Helmbrecht,[2] A. van der Weijden,[2] S. W. van Dongen,[2] I. Schuringa,[2] J. Borchert,[1,2] E. Alarcón-Lladó,[2] W. L. Noorduin,[2,3,a)] and B. Ehrler[2,a)]

AFFILIATIONS

[1]Cavendish Laboratory, University of Cambridge, Cambridge CB2 1TN, United Kingdom
[2]Center for Nanophotonics, AMOLF, Science Park 104, 1098 XG Amsterdam, The Netherlands
[3]Van't Hoff Institute for Molecular Sciences, University of Amsterdam, Amsterdam 1090 GD, The Netherlands

Note: This paper is part of the APL Special Collection on New Solution-processed Perovskites and Perovskite-inspired Optoelectronic Materials and Devices.
[a)]**Authors to whom correspondence should be addressed:** noorduin@amolf.nl and ehrler@amolf.nl

ABSTRACT

In recent years, two dimensional (2D) perovskites have attracted growing interest as a material for optoelectronic applications, combining the defect tolerance and strong absorption of bulk perovskites with enhanced material stability. Moreover, the possibility to tune their bandgap via control of the thickness of the perovskite layers allows precise optimization of the energy levels in these materials, making them ideal candidates for rationally designed semiconductor heterojunctions. However, despite the advances in the synthesis of 2D perovskites, typical fabrication strategies produce either uniform thin-films or isolated single crystals, severely hindering the prospect of patterning these materials. We demonstrate an ion-exchange synthesis of 2D perovskites, starting from a lead carbonate host material and converting it to 2D perovskites via a solution-based treatment. The process allows for the fabrication of 2D perovskites spanning a range of halide compositions and 2D layer thicknesses and yields highly crystalline luminescent materials. We demonstrate the potential of this approach for 2D perovskite patterning, spatially localizing 2D perovskite structures via the conversion of pre-patterned lead carbonate structures. These results significantly expand the possibilities of 2D perovskite material design toward controllable integration of 2D perovskites in complex device architectures.

In recent years, lead halide perovskites have emerged as a promising class of semiconducting materials due to their high carrier mobilities, solution-processable fabrication, and low impact of defects on carrier recombination.[1–3] These properties have led to the swift adoption of perovskite materials in optoelectronic devices, exemplified by the steep rise in efficiency of perovskite based solar cells.[4–6] The technological potential of perovskites is held back by serious stability concerns, as perovskites tend to degrade in the presence of moisture, oxygen, heat, and intense illumination, posing a great challenge to the adoption of perovskite-based devices.[7–9]

Within the family of lead halide perovskite materials, two-dimensional (2D) perovskites have attracted considerable research attention due to their increased material stability.[10–13] 2D perovskites are composed of layers of lead halide octahedra separated by long organic cations, as shown in Fig. 1(a). The layered structure of the material induces quantum confinement of carriers inside the 2D layers, leading to a bandgap energy that depends on the thickness of the 2D layers.[14] Furthermore, the hydrophobic nature of the organic cations that are used to induce the layering of the perovskite structure imparts hydrophobic properties to the material, resulting in increased stability to ambient conditions[15–17] and prompting the integration of 2D perovskites in optoelectronic device architectures.[18–23]

While solution-based spin-coating approaches are well-suited to make planar architectures, patterning processes for perovskites have encountered more difficulties, as these materials are not compatible with typical solvents employed in lithographic fabrication steps.[24–26] Notably, work on the patterning of 2D perovskite materials is scarce and is so far limited to micrometer-sized structures obtained via soft-lithography approaches.[27] The limitations of the current patterning

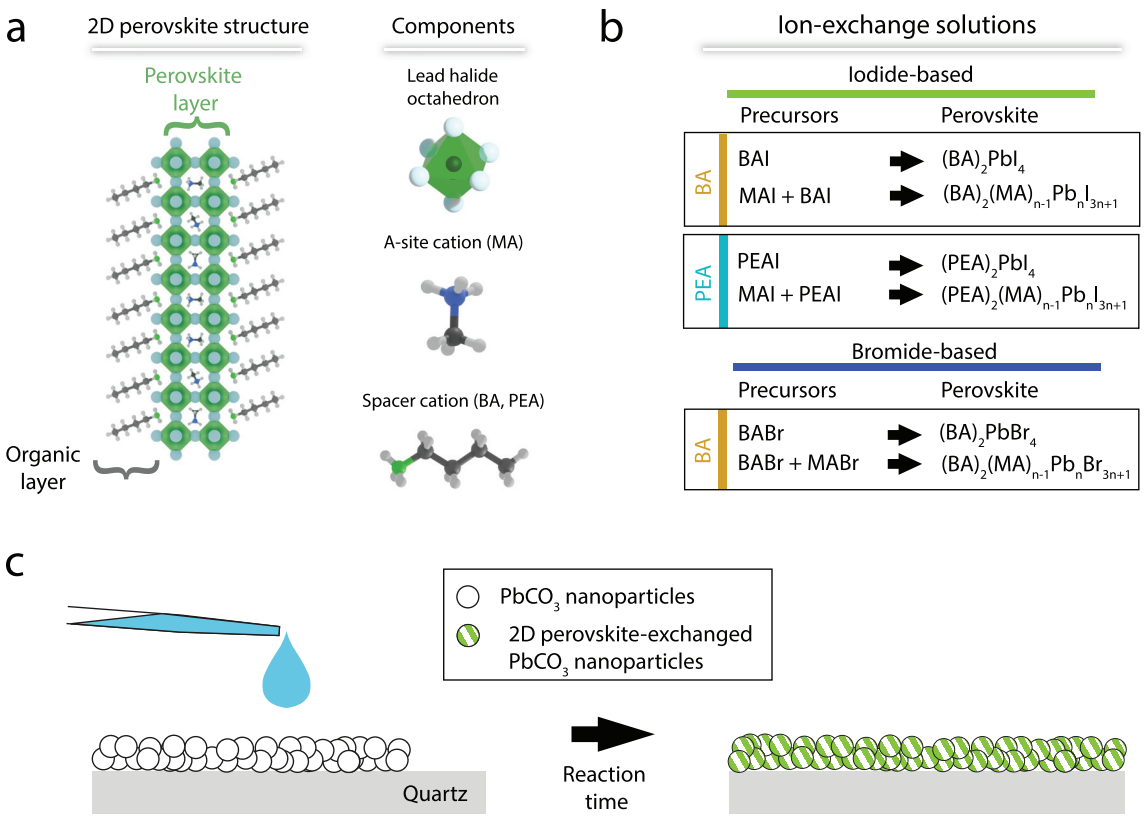

FIG. 1. (a) Schematic of a 2D perovskite layer: the lead halide octahedra and A-site cations, forming the perovskite layer; the spacer cations, forming the insulating organic layers between the perovskite layers. (b) Summary of the different material treatments employed in the study together with the expected perovskite structures. (c) Schematic of the $PbCO_3$ nanoparticle ion-exchange treatment.

approaches highlight the need for novel fabrication strategies, which can more easily incorporate patterning steps.

Recently, ion-exchange reactions have been used to obtain bulk (3D) perovskites of different compositions starting from lead carbonate ($PbCO_3$) materials.[28,29] The method yields 3D perovskite materials with narrow emission and is shown to preserve the morphology and crystallinity of microscale carbonate structures. Moreover, the method is compatible with imprint lithography techniques, allowing in-plane patterning of 3D perovskite materials.[29] These results demonstrate a facile route to robust patterning of perovskite materials, decoupling the patterning of the structure from the formation of the perovskite material. While the generality of the ion-exchange method suggests it could be applied to fabricate lead-containing perovskites of different compositions, it has so far only been employed for the fabrication of 3D methylammonium and formamidinium lead halide perovskites, offering limited energy tunability and control over the stability of the resulting material.

Here, we introduce a $PbCO_3$ conversion method to fabricate 2D perovskites, greatly expanding the range of material systems and material properties obtainable with this ion-exchange approach. The method allows fabrication of luminescent and highly crystalline 2D perovskites with different halide compositions, different organic cations, and different distributions of 2D perovskite thicknesses. The sequential nature of the method, involving the deposition of a host material and its conversion to 2D perovskites, lends itself to different patterning approaches and can be employed to construct complex microstructures with 2D perovskites.

The 2D perovskite structure contains layers of the perovskite material, i.e., a cage of lead halide octahedra with small organic cations (A-site cations) fitting in the voids of the structure and layers of long insulating cations (spacer cations) separating the perovskite layers [Fig. 1(a)]. In order to form a 2D perovskite phase starting from a $PbCO_3$ host material, the halide species, the spacer cation, and optionally the A-site cation need to be delivered to the $PbCO_3$ structure. To do so, we dissolved appropriate organo-halide salts in isopropanol and exposed $PbCO_3$ nanoparticle films to the solution (see the supplementary material, Sec.s S1 and S2).

Butylammonium halide (BAX with X = I, Br) and phenetylammonium halide (PEAX with X = I, Br) salts, providing the butylammonium (BA) and phenetylammonium (PEA) spacer molecules, are widely employed as precursors for 2D perovskites and are, therefore, good candidates to benchmark the properties of the 2D perovskites resulting from the ion-exchange approach. In the presence of the spacer alone, only monolayers (n = 1) of the 2D perovskite structure can be formed, consisting of a single perovskite octahedron across the layer thickness. If the ion-exchange solution also contains a smaller

cation fitting within the cage of the 3D perovskite structure (A-site cations), then thicker quasi-2D perovskite layers ($n > 1$) can form. We employed methylammonium halide (MAX with X = I, Br) as an A-site cation. Depending on the choice of the salt, a range of different compositions and 2D layer thicknesses can be obtained [see Fig. 1(b)].

To convert the $PbCO_3$ films into 2D perovskites, 200 μl of an ion-exchange solution was pipetted on top of the $PbCO_3$ films in a nitrogen-filled glovebox [see Fig. 1(c)]. The pipetted solution covered the whole 15 × 15 mm substrate, and the volume used was sufficient to ensure that evaporation effects are negligible during the duration of the conversion process (1–4 min). At the end of the conversion process, the excess solution is discarded, and the substrate is immersed in fresh isopropanol to remove unused precursors from the surface of the film. For the ion-exchange reactions involving BAI, and those involving a mixture of BAI-MAI, a color change is evident at the end of the conversion, suggesting the formation of chemical species with a bandgap in the visible range. The BABr-based ion exchange procedure did not give rise to an appreciable color change, as the 408 nm bandgap for the $(BA)_2PbBr_4$ $n = 1$ perovskite is at the edge of the visible range.[30] Morphological changes in the nanoparticle film surface depended on the ion-exchange conditions, with the BAI-based reaction showing signs of large-scale recrystallization of the material formed, absent in the case of the BAI-MAI exchange (see the supplementary material, Sec. S13 and Fig. S13).

To determine the nature of the materials formed after the ion-exchange exposure, we performed ultraviolet-visible (UV-VIS) absorption measurements. Figure 2(a) shows the absorption spectrum of a $PbCO_3$ film (gray) and the absorption of a $PbCO_3$ film exposed to a BAI ion-exchange solution for 2 min. While the unexposed $PbCO_3$ film has no absorption in the visible range, the film exposed to BAI has an excitonic peak at the absorption onset, at a wavelength closely matching the expected absorption peak for $n = 1$ $(BA)_2PbI_4$ 2D perovskite[11] (510 nm, vertical line). Photoluminescence (PL) spectra, obtained from the same film, show the presence of a narrow emission peak at the energy of the 2D perovskite band-to-band emission. Figure 2(b) shows a similar plot for 2 min BABr conversion, resulting in an excitonic peak centered at the expected exciton energy for $n = 1$ $(BA)_2PbBr_4$ 2D perovskite[31] (398 nm, vertical line). The presence of the absorption and emission peaks at the bandgap energies of the I-based and Br-based $n = 1$ 2D perovskites indicates the formation of the $n = 1$ 2D perovskite phases as a result of the BAI-based and BABr-based ion-exchange treatments.

Further evidence of the formation of the 2D perovskite phases can be obtained by measuring x-ray diffraction (XRD) of the converted films. Figure 2(c) shows the XRD signal from a sample before and after exposure to the BAI ion-exchange solution, highlighting the appearance of sharp diffraction peaks at low angles. The dominant diffraction peak is located at a $2^*\theta$ value of 6.42°, corresponding to a periodicity of 1.38 nm. This value closely matches the inter-layer distances expected for periodic stacks of 2D perovskite layers.[11] The sharp nature of the peak suggests the formation of large crystallites of stacked 2D perovskite layers. Using the Scherrer equation to obtain a rough estimate of the crystallite size, we obtain a value of 63 nm, suggesting the formation of an extended crystalline domain within the ~100 nm sized $PbCO_3$ NPs (see the supplementary material, Figure S1). The presence of another diffraction peak at 5.77° is associated with residual BAI (see the supplementary material, Sec. S8 and Fig. S8). In contrast to the strong changes observed at low angles, the XRD signal for $2^*\theta > 10°$ remains mostly unchanged. In particular, the XRD peak at 25°, associated with the $PbCO_3$ cerussite (111) peak,[32] is left unchanged by the ion-exchange exposure. This evidence suggests that despite the formation of crystalline 2D perovskite domains, part of the film remains unconverted for the conversion duration used in our study.

The XRD signal obtained from the BABr-exposed $PbCO_3$ film reveals a similar picture, characterized by no changes in the signal at $2^*\theta > 15$ degrees and the appearance of a sharp diffraction peak at 6.45° (1.369 nm), matching closely the value obtained for the BAI-exposed film. The similarity between the peaks in the Br- and I-treated samples is expected in the case of the formation of ordered stacks of 2D perovskite layers, as both treatments should result in butylammonium cations separating the 2D layers. The width of the diffraction peaks provides an estimate for the size of the crystallites of 79 nm. In the BABr-treated sample, it is also possible to see the presence of a second-order diffraction peak associated with the stacks of 2D layers, appearing at 12.89°. Overall, the combined evidence of UV-Vis and XRD data demonstrates that the ion-exchange treatment converts part of the $PbCO_3$ in the films into highly crystalline domains of $(BA)_2PbI_4$ 2D perovskite (BAI-treatment) and $(BA)_2PbBr_4$ 2D perovskite (BABr-treatment).

In addition to the fabrication of monolayer ($n = 1$) 2D perovskite materials, introducing MA-halide precursors into the ion-exchange solution allows for the growth of both $n = 1$ 2D layers and $n > 1$ quasi-2D layers. In our approach, we added a MA-halide salt to a BA-halide ion-exchange solution and performed the ion-exchange exposure as for the BAI and BABr treatments. Additionally, we characterized the effect of skipping the isopropanol washing step to allow long-term exposure of the film with perovskite precursors remaining on the sample surface after the evaporation of the solvent.

Figure 3(a) shows the absorption spectra of a film treated with the BAI+MAI ion-exchange solution either washed (blue trace) or unwashed (green trace). Both traces show the appearance of several peaks in the absorption spectrum, with the washed sample displaying an absorption onset extending toward the bandgap energy of the 3D $MAPbI_3$ perovskite, suggesting the presence of a 3D perovskite phase mixed with the 2D phase. Taking the second derivative of the absorption spectra [Fig. 3(b)] reveals that the wavelengths of the observed peaks match those of the excitonic peaks of different n-values $(BA)_2(MA)_{n-1}Pb_nI_{3n+1}$. While the large energy shift expected for the lowest n-values leads to well-separated peaks for $n = 1$–4, higher n values produce overlapping peaks that cannot be resolved from the continuum of 3D perovskite absorption. Similar results are obtained for the samples treated with a mixture of phenetylammonium iodide and MAI and with a mixture of MABr and BABr, with the appearance of absorption peaks at energies associated to the 2D perovskite layers (see the supplementary material, Secs. S11 and S12 and Figs. S11 and S12).

Typically, synthesis of quasi-2D perovskites with $n > 2$ leads to the formation of a distribution of different n-values within the same sample, with phase-pure $n > 2$ 2D perovskite films achievable only via the hydrogen halide solution-based crystallization method.[10,11] Interestingly, the unwashed sample is characterized by a narrower n-value distribution, showing the presence of $n = 1$, 2, and 3 layers, while missing the higher n-value layers and a 3D perovskite absorption (see the supplementary material, Sec. S10 and Fig. S10). This observation

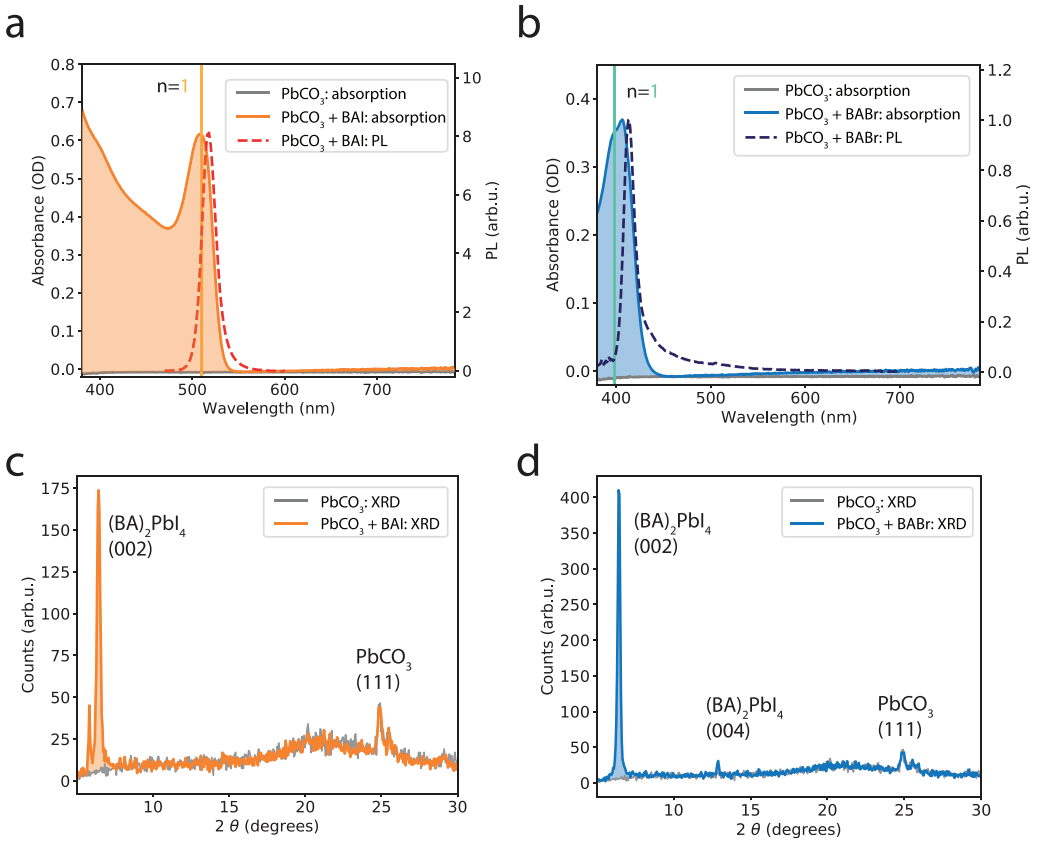

FIG. 2. Absorption and PL spectrum from a $PbCO_3$ film ion-exchanged with BAI (a) and BABr (b), compared to the absorption spectrum of an untreated $PbCO_3$ film (grey traces). [(c) and (d)] XRD measurements performed on a $PbCO_3$ film ion-exchanged with BAI (a) and BABr (b), compared to the signal obtained on an untreated $PbCO_3$ film (grey traces).

suggests that the films continue to react in the solid state, and changes in the time between the drying of the ion-exchanged film and the washing step offer an effective handle to control the distribution of 2D perovskite n-values in the ion-exchanged samples. Similar tuning of the n-values distribution can be achieved changing the exposure time of the ion-exchange treatment (see the supplementary material, Sec. S9 and Fig. S9).

Having demonstrated the formation of 2D perovskites after the ion-exchange procedure, we now further elucidate its chemical pathway. In particular, Holtus *et al.* have shown that the conversion from $PbCO_3$ to 3D perovskites proceeds via a two-step reaction, involving the formation of an amine species and the *in situ* generation of lead iodide, followed by a reaction between lead iodide and excess methylammonium halide.[28] Analogously, we propose the following mechanism for the $PbCO_3$ conversion into 2D perovskites during butylammonium halide treatment:

(1) $PbCO_3 + 2CH_3(CH_2)_3NH_3X \leftrightarrows PbX_2 + H_2O + CO_2 + 2CH_3(CH_2)_3NH_2$,

(2) $PbX_2 + 2CH_3(CH_2)_3NH_3X \leftrightarrows [CH_3(CH_2)_3NH_3]_2PbX_4$.

To validate the proposed reaction scheme, we monitored the formation of the reaction side product butylamine ($CH_3(CH_2)_3NH_2$) using a HPLC-UV (high performance liquid chromatography, coupled to a UV-detector) detection method.[28] The method requires reacting butylamine formed during the reaction with an aldehyde (benzaldehyde), leading to the formation of an imine species [see Fig. 4(a)]. The imine and aldehyde species absorb UV light, each leading to a signal at a distinct retention time in the HPLC measurement [see Figs. 4(b) and S2]. This allows us to differentiate between reacted and unreacted aldehyde molecules, enabling butylamine quantification (see the supplementary material, Sec. S5 and Figs. S2–S5).

Taking aliquots of an ion-exchange solution at different times during the conversion process, then adding the aldehyde to the aliquots and measuring HPLC, we are able to map the dynamics of butylamine formation during the conversion process. Figure 4(c) shows the concentration of butylamine detected in the aliquots as a function of the reaction time. The sudden increase in the butylamine concentration after 1 minute confirms the formation of butylamine and highlights the fast dynamics of the conversion process. The following aliquots show that butylamine formation continues in the 2–4 min range, in line with the increase in material conversion observed in going from 2 to 4 min reaction time (see the supplementary material, Sec. S7 and Figs. S6 and S7).

These results offer insights into the behavior of this 2D synthesis pathway, suggesting strategies for controlling the dynamics of 2D

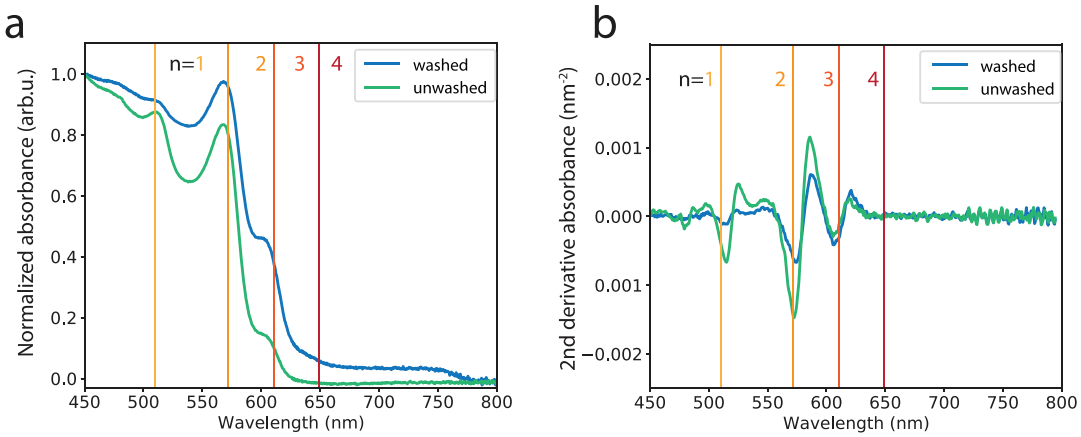

FIG. 3. (a) Absorption spectra of two $PbCO_3$ films ion-exchanged with the MAI-BAI treatment that have either been washed with isopropanol after exchange (blue trace) or left unwashed (green trace). The vertical lines mark the expected bandgap energies for different thicknesses of 2D perovskites. (b) Plot of the second derivative of the absorption spectra shown in panel (a), showing good agreement between the minima of the second derivative and the bandgap energies of 2D perovskites with n-values between 1 and 3.

perovskite formation in the reaction. We note that adding the aldehyde to the ion-exchange solution during the $PbCO_3$ exposure would push the reaction toward the formation of the butylamine product and could be used as a way to alter the relative rate of the two steps of the reaction.

Aside from providing high-quality 2D perovskite materials, the ion-exchange fabrication route also presents advantages for patterning and structuring of perovskite materials. The two-step nature of the fabrication, involving the formation of a robust $PbCO_3$ host and its subsequent conversion into a perovskite material, allows for a facile conversion of complex $PbCO_3$ structures into perovskites, avoiding the difficulties of patterning delicate perovskite materials.[28] We demonstrate the possibility of using the ion-exchange to obtain complex 2D-perovskite-containing microstructures, starting from self-assembled coral-shaped $BaCO_3$ structures (see the supplementary material, Sec. S3), ion-exchanging them into $PbCO_3$,[28] and finally ion exchanging them into 2D perovskites. Following the previous work on the conversion of $PbCO_3$ structures into 3D perovskites, we performed the 2D perovskite exchange via a vapour-phase version of the treatment (see the supplementary material, Secs. S4 and S14 and Fig. S14). Figures 5(a) and 5(b) show a scanning electron microscopy (SEM) picture of a $PbCO_3$ coral-shaped structure before (a) and after (b) the vapour-phase version of the treatment with MABr + BABr. The shape and fine details of the original $PbCO_3$ structure are left mostly unchanged by the ion-exchange process, while energy dispersion spectroscopy (EDS) confirms virtually complete conversion [Fig. 5(c)].

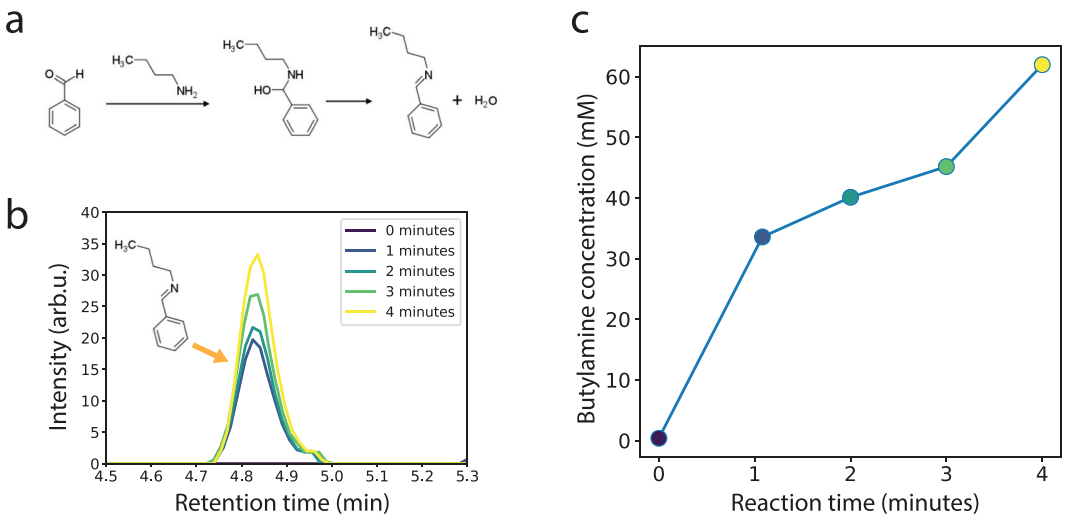

FIG. 4. (a) Scheme representing the reaction between benzaldehyde and butylamine, leading to the formation of an imine species. (b) Chromatograms comparing the ion-exchange solution before exposing it to $PbCO_3$ to aliquots taken from the ion-exchange solution at different exposure times during the reaction, showing an increase in the signal from the imine species. (c) Plot of the concentration of the butylamine species in the aliquots as a function of the reaction time.

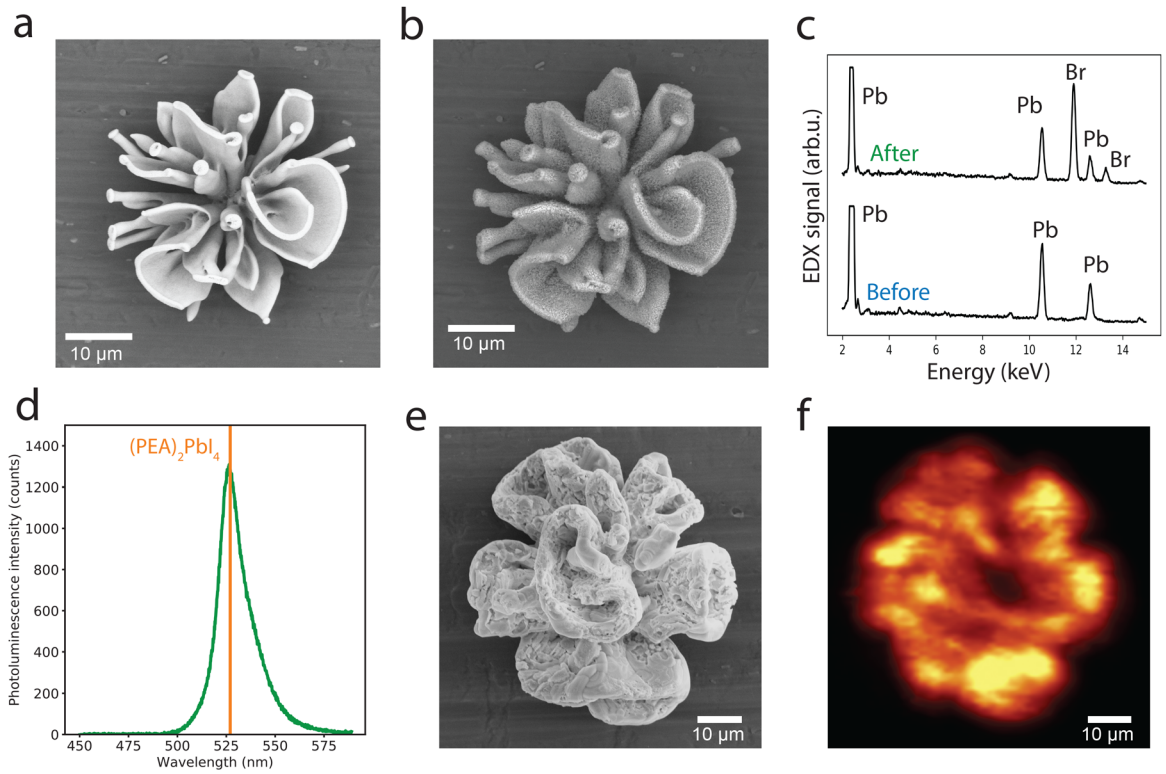

FIG. 5. [(a) and (b)] SEM pictures of a $PbCO_3$ microstructure before (a) and after (b) MABr+BABr ion-exchange performed in the vapour-phase. (c) EDS graph before and after ion-exchange. (d) Photoluminescence spectrum of an ion-exchanged microstructure (vapour-phase PEAI exchange), showing an emission centered at the bandgap energy of the n = 1 $(PEA)_2PbI_4$ 2D perovskite. (e) SEM image and (f) photoluminescence map from the structure whose spectrum is shown in panel (d). The colorscale in panel (f) shows the emission intensity in the 515–535 nm range, revealing localization of the emission on the microstructure.

Figure 5(d) shows a PL spectrum from a structure converted with vapour-phase PEAI treatment, highlighting the presence of a PL maximum around 525 nm, associated with emission from the $(PEA)_2PbI_4$ 2D perovskite material. Figures 5(e) and 5(f), respectively, show an SEM image and a PL map obtained on the PEAI-exchanged coral-like structure whose PL spectrum is shown in Fig. 5(d). The colormap shows the intensity of the emission in the 515–535 nm range as a function of the position, indicating a localization of the emission of the 2D perovskites on the $PbCO_3$ structures. Similar results are obtained converting $PbCO_3$ structures via the solution-based version of ion-exchange treatment (see the supplementary material, Sec. S15 and Fig. S15). These results show that the conversion of complex $PbCO_3$ structures is easily extensible to 2D perovskites, opening the door for complex design of 2D perovskite microstructures.

In conclusion, we have demonstrated that an ion-exchange reaction mechanism can be successfully applied to the fabrication of 2D perovskites, obtaining luminescent materials with high crystallinity, tunable dimensionality, and different halide compositions. The range of materials obtained allows extending the bandgap tunability of 3D perovskites further, while benefiting from the well-known stability increase associated with 2D perovskites. Furthermore, the ion-exchange process unlocks a wide range of patterning strategies for 2D perovskites, as demonstrated by our fabrication of coral-like microstructures of 2D perovskite heterojunctions. The results demonstrate the potential of the proposed method to incorporate 2D perovskites in complex structures and device architectures, paving the way for novel 2D perovskite optoelectronic devices.

See the supplementary material for information on the fabrication of $PbCO_3$ NP films, fabrication of $PbCO_3$ microstructures, ion-exchange procedures, HPLC characterization of ion-exchange kinetics, characterization techniques, the effect of ion-exchange time on material conversion, the XRD signal from unreacted BAI precursor, the effect of ion-exchange time and washing steps on layer thickness distribution in MAI+BAI-treated samples, the PL signal from MABr+BABr-treated and MAI+PEAI-treated $PbCO_3$ NP films, the effect of ion-exchange treatments on $PbCO_3$ NP film morphology, the PL signal from vapour-phase MABr+BABr-exchanged microstructures, and PL maps from liquid-phase MABr+BABr-exchanged microstructures.

The work of G.G. and J.B. was supported by the EPSRC International Centre to Centre under Grant No. EP/S030638/1. A.V.D.W. and W.L.N. acknowledge the Vernieuwingsimpuls Vidi research program "Shaping up materials" with Project No. 016.Vidi.189.083, which is partly financed by the Dutch Research Council (NWO). S.V.D. acknowledges OCENW.KLEIN.155, which is financed by the Dutch Research Council (NWO). D.A. and E.A.-L.

acknowledge the D3N project (Project No. 17972 of the research programme HTSM2019 from the NWO-TTW Domain), which is (partly) financed by the Dutch Research Council (NWO). I.S. acknowledges OCENW.KLEIN.076, which is financed by the Dutch Research Council (NWO).

AUTHOR DECLARATIONS

Conflict of Interest

The authors declare no conflict of interest.

DATA AVAILABILITY

The data that support the findings of this study are available from the corresponding authors upon reasonable request.

REFERENCES

[1]C. Wehrenfennig, M. Liu, H. J. Snaith *et al.*, "Charge-carrier dynamics in vapour-deposited films of the organolead halide perovskite $CH_3NH_3PbI_{3-x}Cl_x$," Energy Environ. Sci. **7**, 2269–2275 (2014).
[2]M. B. Johnston and L. M. Herz, "Hybrid perovskites for photovoltaics: Charge-carrier recombination, diffusion, and radiative efficiencies," Acc. Chem. Res. **49**, 146–154 (2016).
[3]S. D. Stranks, V. M. Burlakov, T. Leijtens *et al.*, "Recombination kinetics in organic-inorganic perovskites: Excitons, free charge, and subgap states," Phys. Rev. Appl. **2**, 034007 (2014).
[4]J. Y. Kim, J.-W. Lee, H. S. Jung *et al.*, "High-efficiency perovskite solar cells," Chem. Rev. **120**, 7867–7918 (2020).
[5]H.-S. Kim, C.-R. Lee, J.-H. Im *et al.*, "Lead iodide perovskite sensitized all-solid-state submicron thin film mesoscopic solar cell with efficiency exceeding 9%," Sci. Rep **2**, 591 (2012).
[6]M. M. Lee, J. Teuscher, T. Miyasaka *et al.*, "Efficient hybrid solar cells based on meso-superstructured organometal halide perovskites," Science **338**, 643–647 (2012).
[7]Y. Rong, Y. Hu, A. Mei *et al.*, "Challenges for commercializing perovskite solar cells," Science **361**, eaat8235 (2018).
[8]J. A. Christians, P. A. Miranda Herrera, and P. V. Kamat, "Transformation of the excited state and photovoltaic efficiency of $CH_3NH_3PbI_3$ perovskite upon controlled exposure to humidified air," J. Am. Chem. Soc. **137**, 1530–1538 (2015).
[9]D. Li, S. A. Bretschneider, V. W. Bergmann *et al.*, "Humidity-induced grain boundaries in $MAPbI_3$ perovskite films," J. Phys. Chem. C **120**, 6363–6368 (2016).
[10]D. H. Cao, C. C. Stoumpos, O. K. Farha *et al.*, "2D homologous perovskites as light-absorbing materials for solar cell applications," J. Am. Chem. Soc. **137**, 7843–7850 (2015).
[11]C. C. Stoumpos, D. H. Cao, D. J. Clark *et al.*, "Ruddlesden–Popper hybrid lead iodide perovskite 2D homologous semiconductors," Chem. Mater. **28**, 2852–2867 (2016).
[12]H. Tsai, W. Nie, J.-C. Blancon *et al.*, "High-efficiency two-dimensional Ruddlesden–Popper perovskite solar cells," Nature **536**, 312–316 (2016).
[13]Y. Chen, Y. Sun, J. Peng *et al.*, "Tailoring organic cation of 2D air-stable organometal halide perovskites for highly efficient planar solar cells," Adv. Energy Mater. **7**, 1700162 (2017).
[14]K. Tanaka and T. Kondo, "Bandgap and exciton binding energies in lead-iodide-based natural quantum-well crystals," Sci. Technol. Adv. Mater. **4**, 599–604 (2003).
[15]H. Zheng, G. Liu, L. Zhu *et al.*, "the effect of hydrophobicity of ammonium salts on stability of quasi-2D perovskite materials in moist condition," Adv. Energy Mater. **8**, 1800051 (2018).
[16]Y. Gao, E. Shi, S. Deng *et al.*, "Molecular engineering of organic–inorganic hybrid perovskites quantum wells," Nat. Chem. **11**, 1151–1157 (2019).
[17]D. Yao, C. Zhang, S. Zhang *et al.*, "2D–3D mixed organic–inorganic perovskite layers for solar cells with enhanced efficiency and stability induced by n-propylammonium iodide additives," ACS Appl. Mater. Interfaces **11**, 29753–29764 (2019).
[18]M. Yuan, L. N. Quan, R. Comin, *et al.*, "Perovskite energy funnels for efficient light-emitting diodes," Nat. Nanotechnol. **11**, 872–877 (2016).
[19]S. Teale, A. Proppe, E. H. Jung *et al.*, "Dimensional mixing increases the efficiency of 2D/3D perovskite solar cells," J. Phys. Chem. Lett. **11**, 5115 (2020).
[20]B. Zhao, Y. Lian, L. Cui *et al.*, "Efficient light-emitting diodes from mixed-dimensional perovskites on a fluoride interface," Nat. Electron. **3**, 704 (2020).
[21]Y. Yang, C. Liu, O. A. Syzgantseva *et al.*, "Defect suppression in oriented 2D perovskite solar cells with efficiency over 18% via rerouting crystallization pathway," Adv. Energy Mater. **11**, 2002966 (2021).
[22]Z. Wang, Q. Wei, X. Liu *et al.*, "Spacer cation tuning enables vertically oriented and graded quasi-2D perovskites for efficient solar cells," Adv. Funct. Mater. **31**, 2008404 (2021).
[23]Y. Huang, Y. Li, E. L. Lim *et al.*, "Stable layered 2D perovskite solar cells with an efficiency of over 19% via multifunctional interfacial engineering," J. Am. Chem. Soc. **143**, 3911–3917 (2021).
[24]J. Harwell, J. Burch, A. Fikouras *et al.*, "Patterning multicolor hybrid perovskite films via top-down lithography," ACS Nano **13**, 3823–3829 (2019).
[25]C. Zou, C. Chang, D. Sun *et al.*, "Photolithographic patterning of perovskite thin films for multicolor display applications," Nano Lett. **20**, 3710–3717 (2020).
[26]K. Wang, G. Xing, Q. Song *et al.*, "Micro- and nanostructured lead halide perovskites: From materials to integrations and devices," Adv. Mater. **33**, 2000306 (2021).
[27]M. E. Kamminga, H.-H. Fang, M. A. Loi *et al.*, "Micropatterned 2D hybrid perovskite thin films with enhanced photoluminescence lifetimes," ACS Appl. Mater. Interfaces **10**, 12878–12885 (2018).
[28]T. Holtus, L. Helmbrecht, H. C. Hendrikse *et al.*, "Shape-preserving transformation of carbonate minerals into lead halide perovskite semiconductors based on ion exchange/insertion reactions," Nat. Chem. **10**, 740–745 (2018).
[29]L. Helmbrecht, M. H. Futscher, L. A. Muscarella *et al.*, "Ion exchange lithography: Localized ion exchange reactions for spatial patterning of perovskite semiconductors and insulators," Adv. Mater. **33**, 2005291 (2021).
[30]N. Kawano, M. Koshimizu, Y. Sun *et al.*, "Effects of organic moieties on luminescence properties of organic–inorganic layered perovskite-type compounds," J. Phys. Chem. C **118**, 9101–9106 (2014).
[31]Z. Yuan, Y. Shu, Y. Xin *et al.*, "Highly luminescent nanoscale quasi-2D layered lead bromide perovskites with tunable emissions," Chem. Commun. **52**, 3887–3890 (2016).
[32]A. Sánchez-Navas, O. López-Cruz, N. Velilla *et al.*, "Crystal growth of lead carbonates: Influence of the medium and relationship between structure and habit," J. Cryst. Growth **376**, 1–10 (2013).